Acta Materialia 187 (2020) 103–111

Contents lists available at ScienceDirect

Acta Materialia

journal homepage: www.elsevier.com/locate/actamat

Full length article

In situ study of vacancy disordering in crystalline phase-change materials under electron beam irradiation

Ting-Ting Jiang[a,1], Xu-Dong Wang[a,1], Jiang-Jing Wang[a,b,*], Yu-Xing Zhou[a], Dan-Li Zhang[a], Lu Lu[c], Chun-Lin Jia[c,d], Matthias Wuttig[b,e], Riccardo Mazzarello[f], Wei Zhang[a,g,*]

[a] Center for Advancing Materials Performance from the Nanoscale, State Key Laboratory for Mechanical Behavior of Materials, Xi'an Jiaotong University, Xi'an 710049, China
[b] Institute of Physics IA, JARA-FIT and JARA-HPC, RWTH Aachen University, 52074 Aachen, Germany
[c] The School of Microelectronics, State Key Laboratory for Mechanical Behavior of Materials, Xi'an Jiaotong, University, Xi'an 710049, China
[d] Ernst Ruska-Centre for Microscopy and Spectroscopy with Electrons, Forschungszentrum Jülich GmbH, 52425 Jülich, Germany
[e] Peter Grünberg Institute (PGI 10), Forschungszentrum Jülich GmbH, 52425 Jülich, Germany
[f] Institute for Theoretical Solid-State Physics, JARA-FIT and JARA-HPC, RWTH Aachen University, 52074 Aachen, Germany
[g] Xi'an Jiaotong University Suzhou Institute, Suzhou 215123, China

A R T I C L E I N F O

Article History:
Received 23 October 2019
Revised 10 January 2020
Accepted 21 January 2020
Available online 27 January 2020

Keywords:
Phase-change materials
GeSbTe
Vacancy disordering
Electron beam irradiation
In situ TEM

A B S T R A C T

Unconventionally high amount of atomic vacancies up to more than 10% are known to form in Ge-Sb-Te crystals upon rapid crystallization from the amorphous phase. Upon thermal annealing, an ordering process of these atomic vacancies is observed, triggering a structural transition from the recrystallized rocksalt structure to a stable layered trigonal structure and a transition from insulator to metal. In this work, we demonstrate an opposite vacancy *disordering* process upon extensive electron beam irradiation, which is accompanied by the reverse transition from the stable trigonal phase to the metastable cubic phase. The combined in situ transmission electron microscopy experiments and density functional theory nudged elastic band calculations reveal three transition stages, including (I) the vacancy diffusion in the trigonal phase, (II) the change in atomic stacking, and (III) the disappearance of vacancy-rich planes. The mechanism of vacancy disordering is attributed to kinetic knock-on collision effects of the high-energy electron beam, which prevail over the heating effects.

1. Introduction

Fast and reversible phase transitions in chalcogenide phase-change materials (PCMs) play a key role in next-generation memory and computing chips [1–20]. Ge-Sb-Te compounds, such as $Ge_2Sb_2Te_5$ and $GeSb_2Te_4$, are under active investigation [21–28], not only because they serve as the key element in commercial products [29], but also because they provide a rich platform for fundamental research in materials science, such as disorder-induced phenomena and metal-insulator transitions [30–40]. Upon rapid crystallization from the amorphous phase, Ge-Sb-Te compounds form a cubic rocksalt (cub-) phase [36,41–44], consisting of two sublattices, one of which contains Te atoms, while the other is occupied by Ge atoms, Sb atoms and atomic vacancies in a random fashion. A trigonal (tri-) phase is formed upon further thermal annealing [45–50], which consists of stacking blocks. These blocks consist of alternately stacked Ge/Sb and Te layers and are terminated by Te layers [51-54].

The cub-phase of Ge-Sb-Te compounds contains a huge amount of atomic vacancies, e.g. 12.5% for $GeSb_2Te_4$: such vacancy concentrations are orders of magnitude higher than those found in conventional semiconductors [55,56]. The formation of vacancy clusters results in Anderson localization of electrons [57], making cub-Ge-Sb-Te compounds disorder-induced Anderson insulators [30,31]. Note that, during fast crystallization, a polycrystalline phase is typically formed. Nevertheless, the grain boundary scattering has been shown to affect the transport properties only marginally [58]. The ordering of vacancies into two-dimensional layers upon thermal annealing leads to both a structural transition into the tri-phase and an insulator-to-metal transition [30,31]. Although the two transitions occur in a relatively narrow range of temperature, they are fundamentally different: in particular, the insulator-to-metal transition is an Anderson transition primarily driven by a reduction in intra-grain lattice disorder, not by a change in structure [37,38].

The vacancy ordering process in Ge-Sb-Te crystals was firstly predicted by density functional theory (DFT) calculations [31], and

* Corresponding author.
E-mail addresses: jiangjingwang@mail.xjtu.edu.cn (J.-J. Wang), wzhang0@mail.xjtu.edu.cn (W. Zhang).

[1] These authors contributed equally to this work.

https://doi.org/10.1016/j.actamat.2020.01.043
1359-6454/

was later confirmed by transmission electron microscopy (TEM) experiments upon thermal annealing [36,37] and electron beam irradiation [44]. In this work, we report on in situ TEM observations of a vacancy disordering induced metastabilization from the tri-phase to the cub-phase in crystalline $GeSb_2Te_4$ (GST) thin films upon extensive electron beam irradiation. Structural details are recorded and analyzed along the transition path, and are further compared with DFT calculations, providing a comprehensive view of vacancy-diffusion induced structural metastabilization in crystalline GST thin films.

2. Experimental and simulation details

$GeSb_2Te_4$ films of ~80 nm thickness were deposited with magnetron sputtering on ultra-thin carbon film (~5 nm) TEM grids and were covered by an electron-transparent ZnS-SiO_2 layer. The as-deposited samples were annealed in argon atmosphere (flow rates of 1200 sccm) in a regular tube furnace at 150 °C for 1 hour and 300 °C for 1 hour to obtain cubic and trigonal phases, respectively. Both sets of thin films were found to be poly-crystalline with grains of different crystallographic orientations along the view direction. The in situ electron beam irradiation experiments were performed based on the trigonal sample in a JEOL JEM-2100F TEM operated at 200 kV. The microstructures were characterized by bright-field and high resolution TEM (HRTEM) imaging, selected area electron diffraction (SAED) analysis and fast Fourier transform (FFT) of HRTEM images.

DFT calculations were performed using the Perdew-Burke-Ernzerhof functionals [59] and the projected augmented plane-wave (PAW) pseudopotentials [60] as implemented in the Vienna *ab initio* simulation package (VASP) [61]. The cut-off energy for the plane-wave basis expansion was set to be 400 eV. Self-consistent calculations were carried out with a Gaussian smearing width of 0.05 eV and a convergence tolerance of 1×10^{-6} eV. K-point grids for the Brillouin zone integration were chosen as $3 \times 3 \times 1$. The initial trigonal model contains 21 atomic layers with 12 Ge, 24 Sb and 48 Te atoms. The nudged elastic band (NEB) calculations were performed using the climbing-image NEB (CI-NEB) implementation [62,63] in VASP. The relaxation convergence tolerance for CI-NEB was set to be 0.03 eV/ Å. In the NEB study, the lattice parameters of the supercell were fixed as $L_X = L_y = 2 \times 4.27$ Å and $L_z = 41.87$ Å, corresponding to the experimental values of the cub-phase, which are very close to that of the trigonal phase with a_{tri} = 4.27 Å and c_{tri} = 41.69 Å [42]. A denser k point mesh of $6 \times 6 \times 2$ was tested for a typical diffusion calculation, yielding almost identical results (Figure S1). The van der Waals correction was also tested [64] and shown to slightly enlarge the relevant energy barriers by ~0.05–0.1 eV (Figure S1).

3. Results and discussion

The TEM images of thermally-annealed samples and the atomic models of the tri- and cub-phase are presented in Fig. 1. For the tri-phase (Fig. 1a), most grains show a needle-like morphology (red box). The HRTEM images and corresponding FFT patterns of selected areas show the structural details of the typical $[01\bar{1}0]_t$- and $[0001]_t$-oriented grains. The yellow arrows indicate structural gaps, which are usually referred to as van der Waals (vdW) gaps in literature, although it has been shown recently that weak covalent interactions are present in addition to van der Waals forces [65-67]. For the cub-phase (Fig. 1b), the grains look equiaxial (red box). Two typical crystallographic orientations $[100]_c$ and $[111]_c$ are highlighted. The measured plane spacings are in line with previous measurements on the two crystalline phases of GST [41,42]. It is important to note that the atomic arrangement and lattice parameters in the $(0001)_t$ plane of the tri-phase and the $(111)_c$ plane of the cub-phase are identical [31], as evidenced by the HRTEM images and the corresponding diffraction patterns (yellow box).

Fig. 1c shows the side view of a $2 \times 2 \times 1$ tri-phase model, containing three septuple-layer (SL) blocks and three structural gaps. The compositional Ge/Sb disorder is considered for the cation-like layers with 50% Ge and 50% Sb for the center layer, 25% Ge and 75% Sb for the two outer layers [42]. Each atomic layer occupies one of the three special positions, i.e. "a" = (0, 0), "b" = (2/3, 1/3) and "c" = (1/3, 2/3), of the unit cell (Fig. 1d). Fig. 1e shows a standard cubic supercell, which can also be built along its [111] direction (Fig. 1f), giving very similar structural features as the tri-phase [68]. The major difference comes from the statistical distribution of atomic vacancies on the cation-like layers in the cub-phase. If all the atomic vacancies are arranged into three particular layers, an ordered phase with cubic stacking (o-cub) can be obtained (Fig. 1g). The stacking sequence of the tri-phase is "–*g*-abcabca-*g*-bcabcab-*g*-cabcabc–" (where "g" represents the structural gap), and can be compactly denoted as "–*g*-A-*g*-B-*g*-C–" (Fig. 1c), whereas the o-cub-phase consists of "–*g*-A-*g*-C-*g*-B–" blocks (Fig. 1g).

If the electron beam was focused to a small area (~200 nm in radius) with a high beam intensity of $\sim 1.1 \times 10^{24}$ e m^{-2} s^{-1} (current density $\sim 1.76 \times 10^{13}$ pA cm^{-2}), a gradual structural transition from the tri-phase to the cub-phase was observed as a function of time (Fig. 2). The tri-phase grain in the center of the irradiation area is indexed to be [0001]-oriented from the SAED pattern, which appeared to be darker as compared to the surrounding grains (Fig. 2a). After 45 min irradiation, a clear change of the image contrast of the center tri-phase grain was found, and extra spots appeared in the corresponding SAED pattern, such as $[\bar{1}2\bar{1}0]_t$ and $[\bar{1}016]_t$ (marked by the yellow arrow and circle in Fig. 2b), indicating that the lattice re-oriented in parts of the central grain. Small lattice distortions were also observed, which could be attributed to the effects of strain during the re-orientation process. Further exposure to the electron beam triggered a structural transition to the cub-phase in parts of the irradiated area, as evidenced by the cub-phase spots (marked by white circles) in the SAED pattern in Fig. 2c. After 115 min irradiation, the irradiated area was comprised of small cub-phase grains with multiple lattice orientations (Fig. 2d). The structural features of this irradiation-induced cubic sample closely resemble the thermally-annealed one.

This direct tri-to-cub structural transition path under electron beam irradiation is in contrast to the conventional thermal-induced tri-to-cub path, which consists of a melt-quenched amorphization and then a rapid crystallization process into the cub-phase. The in situ TEM experiments revealed a progressive and continuous structural metastabilization process from the tri-phase to the cub-phase. To assess the structural changes in more detail, we carried out in situ HRTEM characterizations (Fig. 3) of a target tri-phase grain showing the $[0\ 10\ 10\ 3]_t$-orientation, as evidenced by its FFT pattern (Fig. 3a). Under exposure to electron beam irradiation with the same beam intensity of $\sim 1.1 \times 10^{24}$ e m^{-2} s^{-1} over 45 min, the target trigonal grain splits into two parts with different lattice orientations (Fig. 3b). After 85 min irradiation, a phase transition occurred and two cubic phase grains with different orientations appeared (Fig. 3c). At this stage, the structural gaps in the tri-grain with blue boundary were still visible, while they were gradually filled and the tri-grain transformed to a cub-phase grain with multiple intersecting vacancy-rich $(\bar{1}\bar{1}1)_c$ and $(1\bar{1}1)_c$ layers after 100 min irradiation (Fig. 3d). Such intersecting vacancy-rich layers were also observed in cub-phase GST thin films under thermal annealing [36].

To make further analyses on intra-grain structural details, it is advantageous to record the HRTEM images from the side view of the tri- and cub-phase during the whole transition process. We managed to find a suitable grain for this experiment, despite that the constant change of grain orientation under electron beam

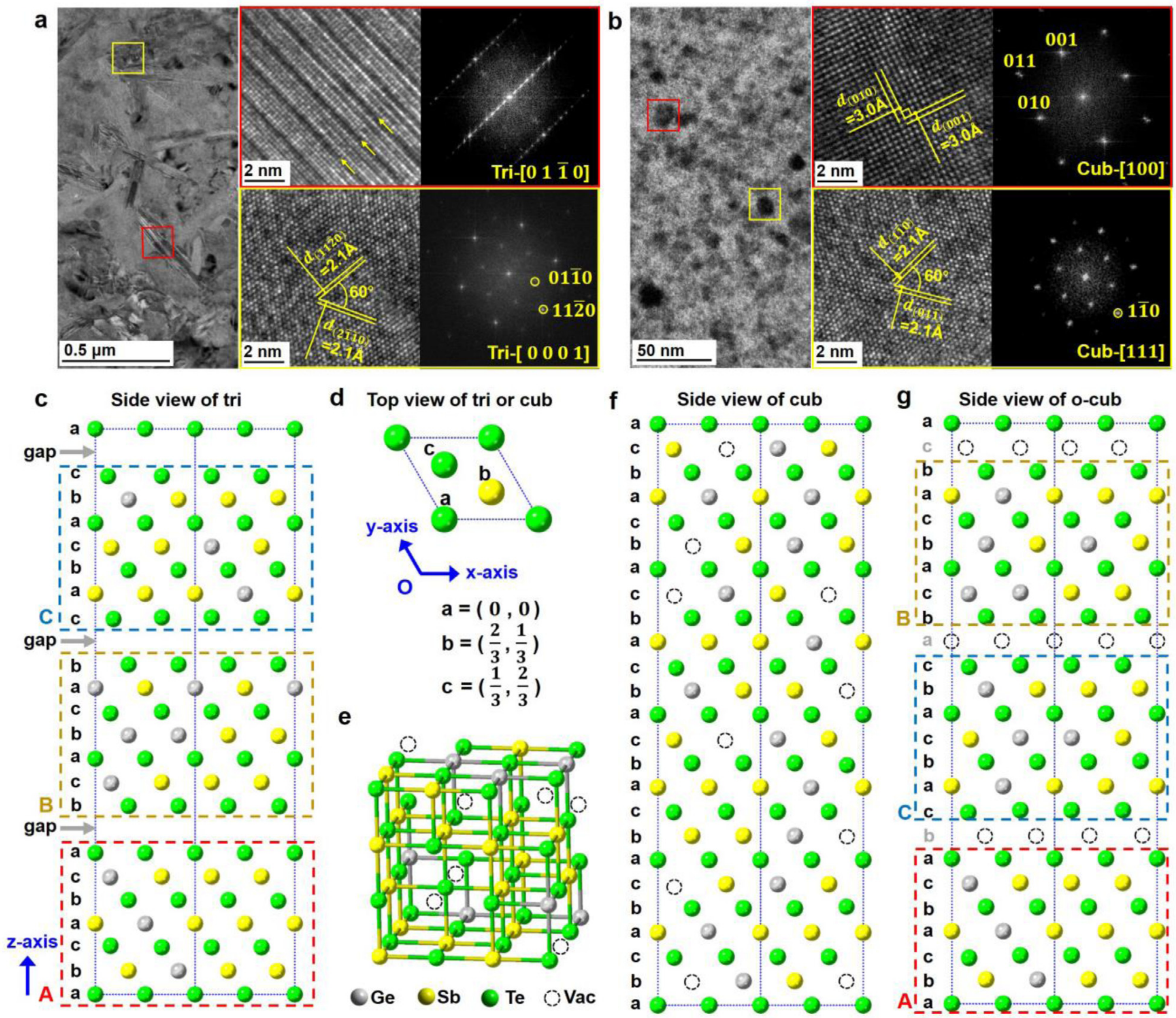

Fig. 1. (**a and b**) The TEM images and the corresponding FFT of the images, showing tri-phase and cub-phase $GeSb_2Te_4$. Grains with typical crystallographic orientations for the two crystalline phases are highlighted. (**c–g**) The atomic models of the two crystalline phases. **c** The side view of the tri-phase, showing three septuple-layer blocks with three structural gaps. Compositional disorder on the cation-like layers is considered. (**d**) The top-view of the three typical in-plane atomic arrangements. (**e and f**) The atomic models of the cub-phase built in a conventional cubic box and in an equivalent orthorhombic box. (**g**) The atomic model of an o-cub-phase with full vacancy layers. (For interpretation of the references to colour in this figure legend, the reader is referred to the web version of this article.)

irradiation. This set of in situ HRTEM recordings is presented in Fig. 4. After 20 min irradiation with the same beam intensity of $\sim 1.1 \times 10^{24}$ e m^{-2} s^{-1}, a mixture of tri-phase and cub-phase structures was observed (Fig. 4a). From these images the stacking sequence of the tri-phase is well distinguished from the cub-phase, marked by yellow and red dots, respectively (Fig. 4a). After 40 min irradiation, the sliding of SL blocks took place (Fig. 4b). Further irradiation could drive the filling of the vacancy-rich $(\bar{1}\bar{1}1)_c$ layers and/or the equivalent $(1\bar{1}1)_c$ layers in the cub-phase structures (Fig. 4c). These vacancy-rich layers were less visible after 100 min irradiation (Fig. 4d), and vanished completely after 130 min irradiation (Fig. 4e). Clearly, this tri-to-cub transition corresponds to a vacancy disordering process, in contrast to the vacancy ordering process upon thermal annealing [31,36].

Next, we performed DFT NEB calculations to study this vacancy disordering induced structural metastabilization process in detail. Within this method, the minimum energy path between known initial and final states is determined by relaxing simultaneously a chain of configurations – denoted as images – connected by springs, which interpolate between the two states. Furthermore, the highest-energy image is made to climb uphill to the saddle point. Starting from a $2 \times 2 \times 1$ tri-phase model, one Sb atom in an outer “cation” layer was moved into the gap region (Fig. 5a). The Sb atom firstly broke six Sb-Te bonds, diffused across a Te layer and then formed six new Sb-Te bonds when it arrived in the gap region, raising the total energy of the system by ~1.0 eV. Three such transitions were calculated in a sequential way, and the barrier for each transition was calculated to be ~1.5 eV (Fig. 5b), higher than the Sb diffusion barrier (~1.0 eV) in cub-phase of GST [36,52]. These high energy barriers for diffusion are important to retain the respective crystalline phases, otherwise, structural transition may already take place spontaneously at low temperatures. The out-of-plane diffusion process created one atomic vacancy in the SL block and turned the structural gap into a vacancy-rich layer. Following our previous definition of vacancy concentration on three target layers l_{vac}, this process can be termed as a tri-100% -> tri-75% transition, representing the Stage I of the whole vacancy disordering process. For the sake of convenience, we abbreviated the three target vacancy-rich layers as VLs.

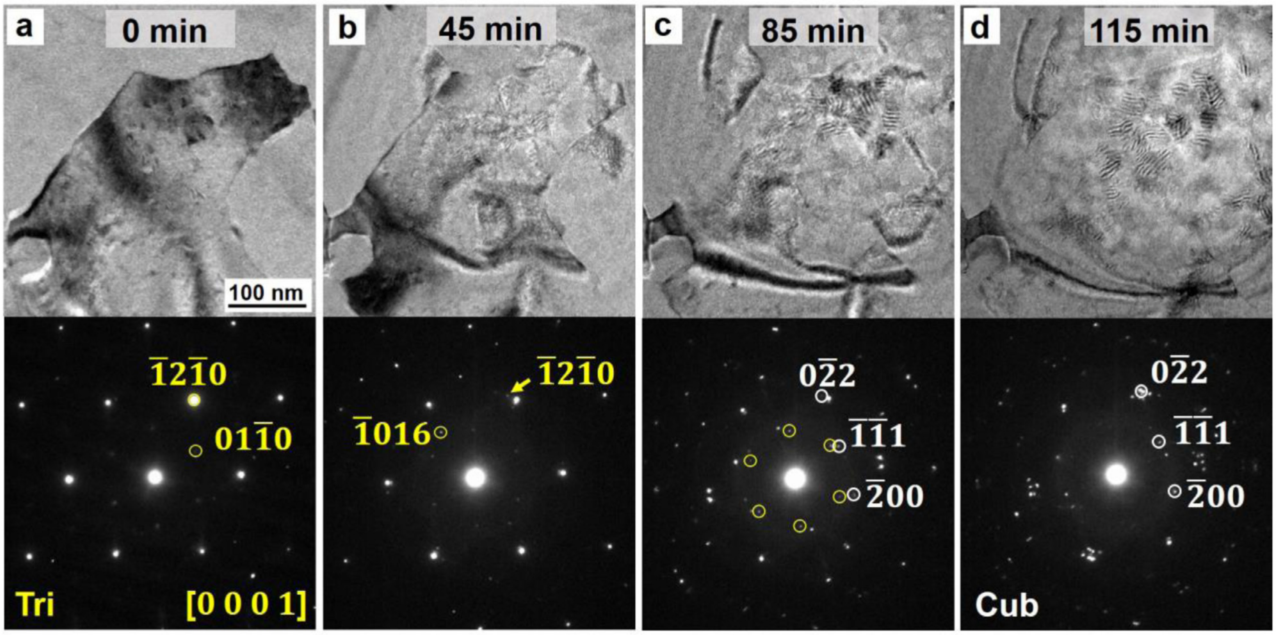

Fig. 2. (**a**) Bright-field TEM image of a thermally-induced tri-phase grain viewed along the $[0001]_t$ direction, as confirmed by the SAED pattern. (**b**) The snapshot and the corresponding SAED pattern of the tri-phase grain after 45 min irradiation. Yellow arrow and circle in the SAED pattern indicate other sets of reflection spots that does not belong to the original $[0001]_t$ zone axis, revealing the re-orientation of part of the grain. The lattice is slightly distorted due to strain effects during the re-orientation process. (**c**) shows a transition from tri- to cub-GST. Both tri- and cub-GST reflection spots can be observed in the SAED pattern, which are marked with yellow and white circles, respectively. **d** All the tri-phase grains transformed into cub-phase. (For interpretation of the references to colour in this figure legend, the reader is referred to the web version of this article.)

According to our previous total energy calculations for large-scale GST models (consisting of 1008 atoms in a $\sim 3.0 \times 2.6 \times 4.2$ nm^3 supercell) [31], for the system with $l_{vac} = 75\%$ the tri-phase stacking is still energetically more favorable than the cubic one, but if l_{vac} lowers to 50%, the cub-phase stacking has a smaller total energy, suggesting a block shifting transition associated with vacancy diffusion [31]. Our small-scale models show the same trends in total energy and enable a direct transition calculation to understand the atomic details involved in this process. To reduce the l_{vac} and obtain the cub-phase stacking, atomic diffusion into vacancy gaps should continue and the shifting of the SL blocks should occur. This tri-75% -> cub-50% transition process represents the Stage II of the whole vacancy disordering process.

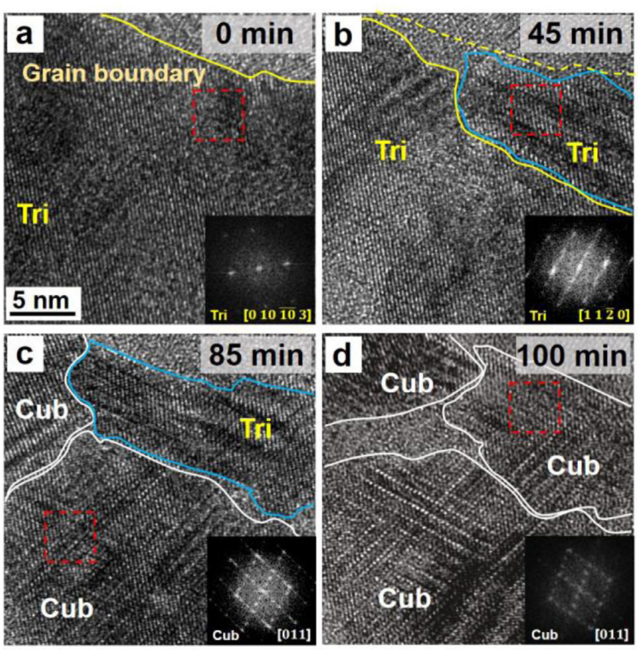

Fig. 3. (**a**) The HRTEM image of a tri-phase grain prior to the extensive irradiation. The FFT pattern corresponding to the area inside the red dashed box indicates the $[0\ 10\ 10\ 3]_t$ orientation of this grain. (**b**–**d**) The snapshots of the metastabilization process after 45, 85 and 100 min irradiation. The dashed yellow line in **b** marks the initial grain boundary. Under irradiation, the tri-phase grain in **a** was divided into two parts firstly, as marked with the yellow and blue lines in **b**. In **c**, two cub-phase grains with different orientations appeared, as confirmed by the FFT pattern. (**d**) All tri-phase grains transformed into the cub-phase with intersecting vacancy-rich layers after 100 min irradiation. (For interpretation of the references to colour in this figure legend, the reader is referred to the web version of this article.)

A typical transition path of Stage II is presented in Fig. 6a: the path can be characterized by three sub-processes, namely, (1) out-of-plane "cation" diffusion, (2) in-plane "cation" diffusion and (3) SL block shifting. The first two peaks in the NEB energy profile (Fig. 6b) correspond to three out-of-plane diffusions and the other peaks correspond to six in-plane diffusions in the three VLs. The barrier for in-plane diffusion is on average ~0.3 eV, which is much smaller than the out-of-plane diffusion barrier of 1.2–1.6 eV. The top two SL blocks shifted continuously during the transition process. The shifting pathway was chosen to be a "snake-like" path (Fig. 6c), i.e. the middle SL block shifted from B position to C position, and the top SL block shifted from C position to another B position. No energy barrier was observed for the continuous block shifting process. If two SL blocks moved towards each other and swapped their position, which is known as an "overhead" path [69,70], a much higher energy barrier would appear. This favorable "snake-like" path is confirmed by a simple block shifting calculation presented in Figure S2.

As shown in Fig. 4, the vacancy disordering process can continue upon extensive electron beam irradiation until vacancy-rich layers vanish, indicative of further atomic diffusion into the vacancy-rich layers. Once this process is completed, the vacancy concentration of all "cation" layers gets close to 25%, and the vacancy-rich layers are no longer distinguishable from other "cation" layers. This cub-50% -> cub-25% transition process represents Stage III of the whole vacancy disordering process. Similar to Stage I, the transition is mainly dominated by out-of-plane atomic diffusion with a barrier

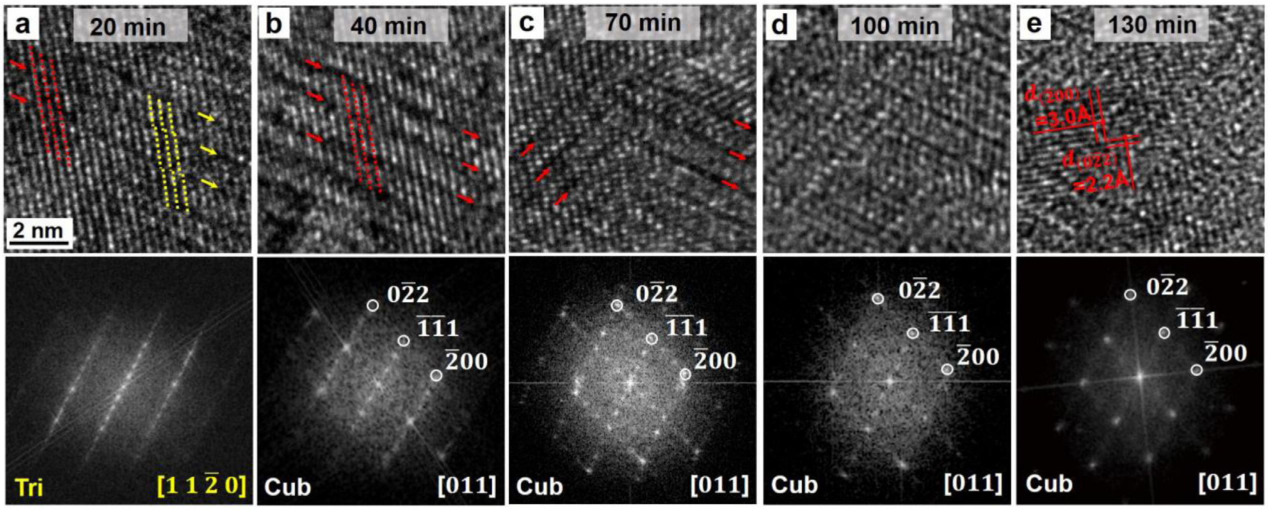

Fig. 4. Series of images of a GST grain and corresponding FFT patterns at different irradiation time. (**a**) The GST grain with mixture of tri-phase (yellow dots) and cub-phase (red dots) stackings formed after 20 min irradiation. Structural gaps and vacancy-rich layers are marked by yellow and red arrows, respectively. (**b**) The shift of SL blocks occurred after 40 min irradiation. **c** Multiple $(\bar{1}\bar{1}1)_c$ and $(1\bar{1}1)_c$ vacancy-rich layers were still present after 70 min irradiation. **d** The vacancy-rich layers were mostly filled after 100 min irradiation. (**e**) The image of the grain after 130 min irradiation. The vacancy-rich layers fully vanished, and atomic vacancies became randomly distributed as in the conventional cub-phase. (For interpretation of the references to colour in this figure legend, the reader is referred to the web version of this article.)

of ~1.7 eV (Fig. 7). Overall, the transition barriers during the whole tri-to-cub structural transition are not very large, and can be triggered by extensive exposure to high-energy electron beams.

In contrast to the vacancy ordering induced structural stabilization process upon thermal annealing, the irradiation-induced structural metastabilization is driven by the kinetic collision effects of electron beams [71], which generate displacement forces to trigger vacancy diffusion. As noted above, to generate tri-to-cub transition using pure thermal effects, the thin films should undergo firstly a melt-quenched amorphization and then recrystallization into the cub-phase. But clearly, in the irradiation experiments, the change in TEM images and corresponding diffraction was continuous, and no sign of abrupt melting was observed.

Starting from the cub-phase, if the thin films were exposed further to the electron beams, a progressive and non-thermal amorphization process would eventually occur [72]. The higher the accelerating voltage, the stronger the kinetic effects of the electron beam, thereby the faster the amorphization transitions [72]. As indicated by Raman spectroscopy monitoring, similar structural metastabilization from the tri-phase to the cub-phase and finally to the amorphous phase were also observed in GST thin films under Ar^+ ions bombardment [40,73], in which the kinetic effects of ion beams were stronger than those of electron beams. The vacancy ordering and disordering process in GST crystals is schematically summarized in Fig. 8.

In addition to kinetic effects, electron beams could also induce specimen heating [74-76] and radiolysis effects [71]. It was shown

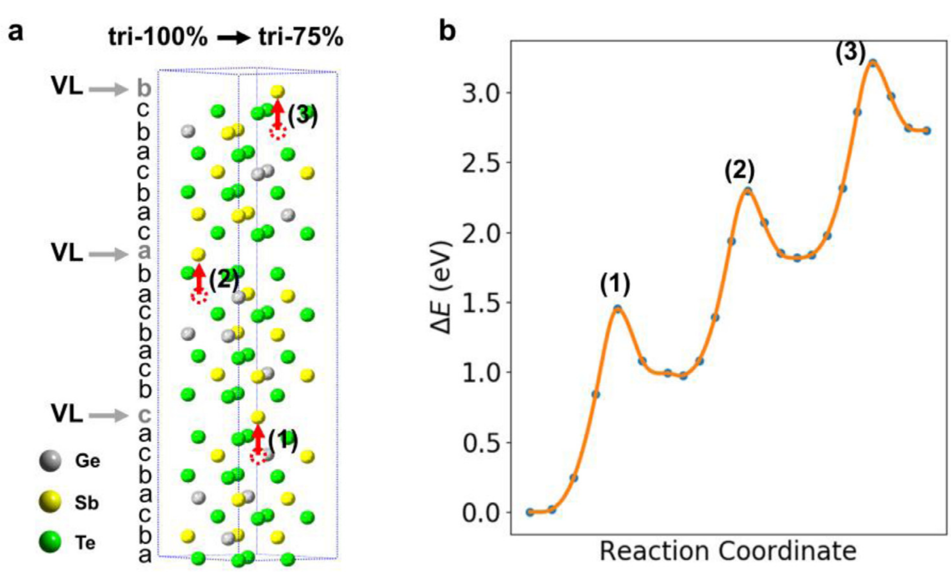

Fig. 5. (**a**) A typical transition path from tri-100% to tri-75% with three Sb atoms moved into their adjacent structural gap regions, respectively, forming three VLs. Dotted circles represent the original positions of the Sb atoms. (**b**) The NEB energy profile of the three atomic diffusion processes described in **a**. Each process raised the total energy of the system by ~1 eV, with an energy barrier of ~1.5 eV.

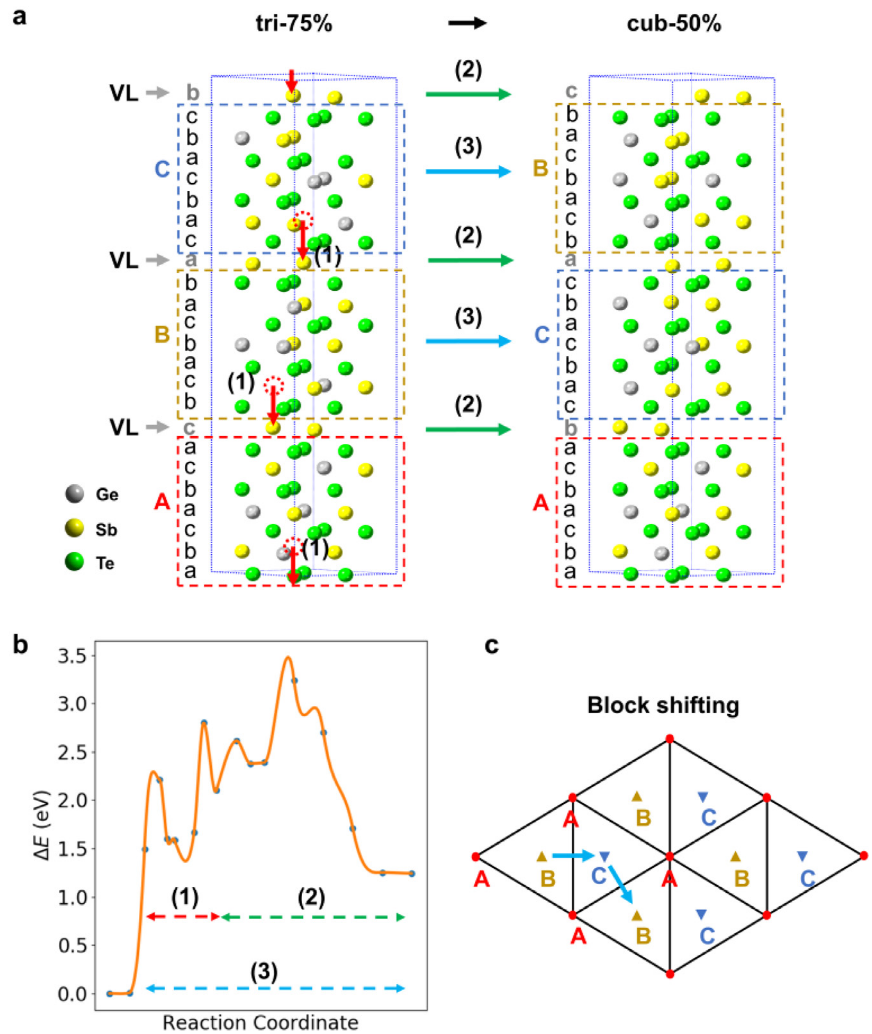

Fig. 6. (**a**) A typical transition path from tri-75% to cub-50% in which three sub-processes occurred simultaneously: (1) out-of-plane "cation" diffusion, (2) in-plane "cation" diffusion, (3) SL block shifting. (**b**) The corresponding NEB energy profile. The first two peaks correspond to out-of-plane "cation" diffusion and the latter peaks correspond to in-plane "cation" diffusion, while the SL blocks shifted continuously during the transition with no obvious energy peak. (**c**) The shifting path of the top two SL blocks. (For interpretation of the references to colour in this figure legend, the reader is referred to the web version of this article.)

that amorphous Ge-Sb-Te and other PCMs thin films could be crystallized using electron beams, where the specimen heating played an important role [77–80]. The heating effects could get stronger

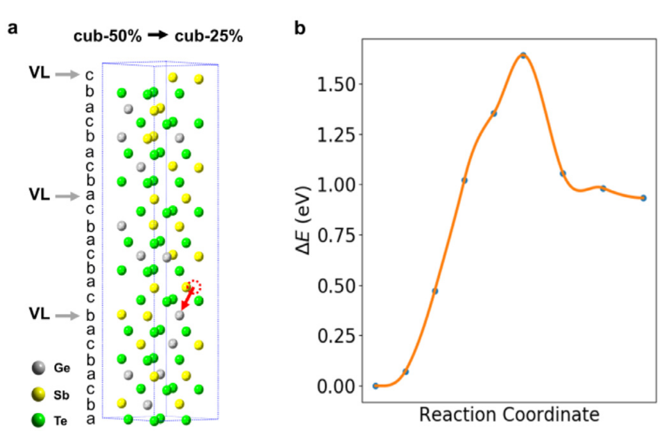

Fig. 7. (**a**) A typical transition path from cub-50% to cub-25%. (**b**) The corresponding NEB energy profile. The energy barrier for the out-of-plane diffusion is ~1.7 eV.

at a lower accelerating voltage [71]. However, the estimated temperature rise here is well below the melting point of GST ($T_m \sim$ 650 °C), which is insufficient to trigger melt-quenching amorphization and then recrystallization into the cub-phase. Indeed, no abrupt structural change was observed during in situ recording of the irradiation-induced metastabilization process, indicating a continuous and non-thermal structural transition from the tri-phase to the cub-phase, in stark contrast with the thermal-induced transitions in GST.

Besides, electron beam irradiation was also shown to tune the size of atomic blocks via vacancy disordering in GeTe-Sb_2Te_3 superlattices [81], or to induce the motion of swapped bilayers, and, thereby, dynamical reconfiguration of structural gaps, in layer-structured Ge-Sb-Te and related materials [82–85]. Due to the multiple effects of electron beams, we therefore note that for the measurement of structural details of a particular solid-state phase of PCMs, the three critical TEM parameters, namely, accelerating voltage, beam intensity and recording time, should be reduced as much as possible to avoid structural transitions during the measurement. However, in order to study the dynamical process of structural transitions in PCMs, these parameters can be tuned at higher values accordingly.

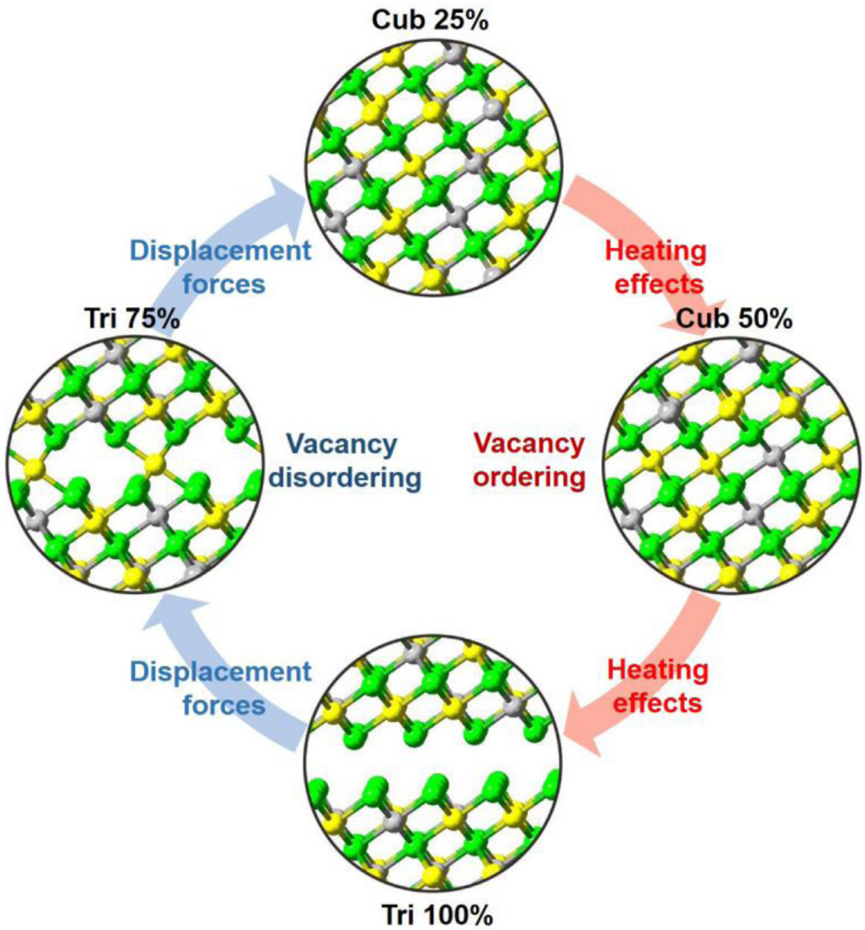

Fig. 8. The schematic of the phase transitions in GST crystals. Vacancy ordering and disordering could be triggered by either heating effects or displacement forces, driving the reverse structural transition between the cub-phase and the tri-phase of GST. (For interpretation of the references to colour in this figure legend, the reader is referred to the web version of this article.)

4. Conclusion

In summary, we have demonstrated a progressive vacancy disordering process that induced a structural transition from the tri-phase to the cub-phase in GST thin films under extensive electron beam irradiation. The in situ TEM recordings provided a comprehensive real-time and real-space view of the vacancy disordering process, while the DFT NEB calculations elucidated the atomic details involved in this transition. In contrast to heating effects that trigger vacancy ordering and structural transition to the stable tri-phase, the electron beam irradiation induces displacement forces driving a reverse metastabilization transition in crystalline GST thin films. It was demonstrated that intra-grain structural changes, in particular, the statistical distribution of atomic vacancies, play a major role in shaping the localization behavior of electrons. Our electron irradiation experiment provides an alternative approach to tune the vacancy distribution that is crucial for the disorder-driven metal-insulator transition of GST crystals.

Declaration of Competing Interest

None.

Acknowledgements

W.Z. thanks the support of National Natural Science Foundation of China (61774123), 111 Project 2.0 (BP2018008), the Science and Technology Department of Jiangsu Province (BK20170414), and the Young Talent Support Plan of Xi'an Jiaotong University. C.-L.J., R.M., and M.W. acknowledge funding from Deutsche Forschungsgemeinschaft within SFB 917 "Nanoswitches." The authors also acknowledge the computational resources provided by the HPC platform of Xi'an Jiaotong University. The authors also acknowledge the support by the Materials Studio for Neuro-inspired Computing (mSonic) and the International Joint Laboratory for Micro/Nano Manufacturing and Measurement Technologies of Xi'an Jiaotong University.

Supplementary materials

Supplementary material associated with this article can be found in the online version at doi:10.1016/j.actamat.2020.01.043.

References

[1] W. Zhang, R. Mazzarello, M. Wuttig, E. Ma, Designing crystallization in phase-change materials for universal memory and neuro-inspired computing, Nat. Rev. Mater. 4 (2019) 150–168.
[2] M. Wuttig, N. Yamada, Phase-change materials for rewriteable data storage, Nat. Mater. 6 (2007) 824–832.
[3] H.-S.P. Wong, S. Raoux, S.B. Kim, J. Liang, J.P. Reifenberg, B. Rajendran, M. Asheghi, K.E. Goodson, Phase change memory, Proc. IEEE 98 (2010) 2201.
[4] A. Sebastian, M. Le Gallo, G.W. Burr, S. Kim, M. BrightSky, E. Eleftheriou, Tutorial: brain-inspired computing using phase-change memory devices, J. Appl. Phys. 124 (2018) 111101.
[5] D. Ielmini, H.-S.P. Wong, In-memory computing with resistive switching devices, Nat. Electron. 1 (2018) 333–343.
[6] Q. Xia, J.J. Yang, Memristive crossbar arrays for brain-inspired computing, Nat. Mater. 18 (2019) 309–323.

[7] W. Zhang, R. Mazzarello, E. Ma, Phase-change materials in electronics and photonics, MRS Bulletin 44 (2019) 686–690.
[8] W. Zhang, M. Wuttig, Phase change materials and superlattices for non-volatile memories, Phys. Status Solidi RRL 13 (2019) 1900130.
[9] F. Rao, K. Ding, Y. Zhou, Y. Zheng, M. Xia, S. Lv, Z. Song, S. Feng, I. Ronneberger, R. Mazzarello, W. Zhang, E. Ma, Reducing the stochasticity of crystal nucleation to enable subnanosecond memory writing, Science 358 (2017) 1423–1427.
[10] K. Ding, J. Wang, Y. Zhou, H. Tian, L. Lu, R. Mazzarello, C. Jia, W. Zhang, F. Rao, E. Ma, Phase-change heterostructure enables ultralow noise and drift for memory operation, Science 366 (2019) 210–215.
[11] F. Rao, W. Zhang, E. Ma, Catching structural transitions in liquids, Science 364 (2019) 1032–1033.
[12] P. Zalden, F. Quirin, M. Schumacher, J. Siegel, S. Wei, A. Koc, M. Nicoul, M. Trigo, P. Andreasson, H. Enquist, M. Shu, T. Pardini, M. Chollet, D. Zhu, H. Lemke, I. Ronneberger, J. Larsson, A.M. Lindenberg, H.E. Fischer, S. Hau-Riege, D.A. Reis, R. Mazzarello, M. Wuttig, K. Sokolowski-Tinten, Femtosecond X-ray diffraction reveals a liquid-liquid phase transition in phase-change materials, Science 364 (2019) 1062–1067.
[13] F. Xiong, A.D. Liao, D. Estrada, E. Pop, Low-power switching of phase-change materials with carbon nanotube electrodes, Science 332 (2011) 568–570.
[14] A.V. Kolobov, P. Fons, A.I. Frenkel, A.L. Ankudinov, J. Tominaga, T. Uruga, Understanding the phase-change mechanism of rewritable optical media, Nat. Mater. 3 (2004) 703–708.
[15] D. Loke, T.H. Lee, W.J. Wang, L.P. Shi, R. Zhao, Y.C. Yeo, T.C. Chong, S.R. Elliott, Breaking the speed limits of phase-change memory, Science 336 (2012) 1566–1569.
[16] M. Salinga, B. Kersting, I. Ronneberger, V.P. Jonnalagadda, X.T. Vu, M.L. Gallo, I. Giannopoulos, O. Cojocaru-Mirédin, R. Mazzarello, A. Sebastian, Monatomic phase change memory, Nat. Mater. 17 (2018) 681–685.
[17] Q. Zhang, Y. Zhang, J. Li, R. Soref, T. Gu, J. Hu, Broadband nonvolatile photonic switching based on optical phase change materials: beyond the classical figure-of-merit, Opt. Lett. 43 (2018) 94–97.
[18] W. Zhang, E. Ma, Single-element glass to record data, Nat. Mater. 17 (2018) 654–655.
[19] Z. Cheng, C. Ríos, W.H.P. Pernice, C.D. Wright, H. Bhaskaran, On-chip photonic synapse, Sci. Adv. 3 (2017) e1700160.
[20] P.A. Vermeulen, J. Mulder, J. Momand, B.J. Kooi, Strain engineering of van der Waals heterostructures, Nanoscale 10 (2018) 1474–1480.
[21] N. Yamada, E. Ohno, N. Akahira, K. Nishiuchi, K. Nagata, M. Takao, High speed overwritable phase change optical disk material, Jpn. J. Appl. Phys. Part 1 26 (1987) 61–66.
[22] N. Yamada, E. Ohno, K. Nishiuchi, N. Akahira, M. Takao, Rapid-phase transitions of gete-sb2te3 pseudobinary amorphous thin films for an optical disk memory, J. Appl. Phys. 69 (1991) 2849–2856.
[23] Z. Sun, J. Zhou, R. Ahuja, Structure of phase change materials for data storage, Phys. Rev. Lett. 96 (2006) 055507.
[24] S. He, L. Zhu, J. Zhou, Z. Sun, Metastable stacking-polymorphism in Ge2Sb2Te5, Inorg. Chem. 56 (2017) 11990–11997.
[25] M. Xu, Y. Cheng, H. Sheng, E. Ma, Nature of atomic bonding and atomic structure in the phase-change Ge2Sb2Te5 glass, Phys. Rev. Lett. 103 (2009) 195502.
[26] Xian-Bin Li, Nian-Ke Chen, Xue-Peng Wang, H.-B. Sun, Phase-Change superlattice materials toward low power consumption and high density data storage: microscopic picture, working principles, and optimization, Adv. Funct. Mater. 28 (2018) 1803380.
[27] I. Ronneberger, W. Zhang, H. Eshet, R. Mazzarello, Crystallization properties of the Ge2Sb2Te5 phase-change compound from advanced simulations, Adv. Funct. Mater. 25 (2015) 6407–6413.
[28] X.-P. Wang, X.-B. Li, N.-K. Chen, Q.-D. Chen, X.-D. Han, S. Zhang, H.-B. Sun, Element-specific amorphization of vacancy-ordered GeSbTe for ternary-state phase change memory, Acta Mater. 136 (2017) 242–248.
[29] J. Choe, Intel 3D XPoint memory die removed from intel optane^{TM} pcm (Phase change memory). http://www.techinsights.com/about-techinsights/overview/blog/intel-3D-xpoint-memory-die-removed-from-intel-optane-pcm/).
[30] T. Siegrist, P. Jost, H. Volker, M. Woda, P. Merkelbach, C. Schlockermann, M. Wuttig, Disorder-induced localization in crystalline phase-change materials, Nat. Mater. 10 (2011) 202–208.
[31] W. Zhang, A. Thiess, P. Zalden, R. Zeller, P.H. Dederichs, J.Y. Raty, M. Wuttig, S. Blügel, R. Mazzarello, Role of vacancies in metal-insulator transitions of crystalline phase-change materials, Nat. Mater. 11 (2012) 952–956.
[32] N.P. Breznay, H. Volker, A. Palevski, R. Mazzarello, A. Kapitulnik, M. Wuttig, Weak antilocalization and disorder-enhanced electron interactions in annealed films of the phase-change compound GeSb2Te4, Phys. Rev. B 86 (2012) 205302.
[33] M. Xu, W. Zhang, R. Mazzarello, M. Wuttig, Disorder control in crystalline GeSb2Te4 using high pressure, Adv. Sci. 2 (2015) 1500117.
[34] M. Xu, Z. Yu, L. Wang, R. Mazzarello, M. Wuttig, Reversing the resistivity contrast in the phase−change memory material GeSb2Te4 using high pressure, Adv. Electron. Mater. 1 (2015) 1500240.
[35] W. Zhang, M. Wuttig, R. Mazzarello, Effects of stoichiometry on the transport properties of crystalline phase-change materials, Sci. Rep. 5 (2015) 13496.
[36] B. Zhang, W. Zhang, Z.-J. Shen, Y.-J. Chen, J.-X. Li, S.-B. Zhang, Z. Zhang, M. Wuttig, R. Mazzarello, E. Ma, X.-D. Han, Element-resolved atomic structure imaging of rocksalt Ge2Sb2Te5 phase-change material, Appl. Phys. Lett. 108 (2016) 191902.
[37] V. Bragaglia, F. Arciprete, W. Zhang, A.M. Mio, E. Zallo, K. Perumal, A. Giussani, S. Cecchi, J.E. Boschker, H. Riechert, S. Privitera, E. Rimini, R. Mazzarello, R. Calarco, Metal-Insulator transition driven by vacancy ordering in ZeSbTe phase change materials, Sci. Rep. 6 (2016) 23843.
[38] J.-J. Wang, Y.-Z. Xu, R. Mazzarello, M. Wuttig, W. Zhang, A review on disorder-driven metal-insulator transition in crystalline vacancy-rich GeSbTe phase-change materials, Materials (Basel) 10 (2017) 862.
[39] J. Kim, S.-H. Jhi, Disorder-induced structural transitions in topological insulating Ge-Sb-Te compounds, J. Appl. Phys. 117 (2015) 195701.
[40] S.M.S. Privitera, A.M. Mio, E. Smecca, A. Alberti, W. Zhang, R. Mazzarello, J. Benke, C. Persch, F. La Via, E. Rimini, Structural and electronic transitions in Ge2Sb2Te5 induced by ion irradiation damage, Phys. Rev. B 94 (2016) 094103.
[41] B.J. Kooi, J.T.M. De Hosson, Electron diffraction and high-resolution transmission electron microscopy of the high temperature crystal structures of GexSb2Te3+x (x=1,2,3) phase change material, J. Appl. Phys. 92 (2002) 3584–3590.
[42] T. Matsunaga, N. Yamada, Structural investigation of gesb2te4:a high-speed phase-change material, Phys. Rev. B 69 (2004) 104111.
[43] U. Ross, A. Lotnyk, E. Thelander, B. Rauschenbach, Direct imaging of crystal structure and defects in metastable Ge2Sb2Te5 by quantitative aberration-corrected scanning transmission electron microscopy, Appl. Phys. Lett. 104 (2014) 121904.
[44] A. Lotnyk, S. Bernütz, X. Sun, U. Ross, M. Ehrhardt, B. Rauschenbach, Real-space imaging of atomic arrangement and vacancy layers ordering in laser crystallised Ge2Sb2Te5 phase change thin films, Acta Mater 105 (2016) 1–8.
[45] J. Momand, R. Wang, J.E. Boschker, M.A. Verheijen, R. Calarco, B.J. Kooi, Interface formation of two- and three-dimensionally bonded materials in the case of GeTe-Sb2Te3 superlattices, Nanoscale 7 (2015) 19136–19143.
[46] J. Momand, R. Wang, J.E. Boschker, M.A. Verheijen, R. Calarco, B.J. Kooi, Dynamic reconfiguration of van der Waals gaps within GeTe-Sb2Te3 based superlattices, Nanoscale 9 (2017) 8774–8780.
[47] M. Behrens, A. Lotnyk, J.W. Gerlach, I. Hilmi, T. Abel, P. Lorenz, B. Rauschenbach, Ultrafast interfacial transformation from 2D- to 3D-bonded structures in layered Ge-Sb-Te thin films and heterostructures, Nanoscale 10 (2018) 22946–22953.
[48] Y. Zheng, Y. Wang, T. Xin, Y. Cheng, R. Huang, P. Liu, M. Luo, Z. Zhang, S. Lv, Z. Song, S. Feng, Direct atomic identification of cation migration induced gradual cubic-to-hexagonal phase transition in Ge2Sb2Te5, Commun. Chem. 2 (2019) 13.
[49] A. Lotnyk, T. Dankwort, I. Hilmi, L. Kienle, B. Rauschenbach, Atomic-scale observation of defects motion in van der Waals layered chalcogenide based materials, Scripta Mater 166 (2019) 154–158.
[50] Y. Zheng, Y. Cheng, R. Huang, R. Qi, F. Rao, K. Ding, W. Yin, S. Song, W. Liu, Z. Song, S. Feng, Surface energy driven cubic-to-hexagonal grain growth of Ge2Sb2Te5 thin film, Sci Rep 7 (2017) 5915.
[51] J.-J. Wang, J. Wang, H. Du, L. Lu, P.C. Schmitz, Johannes Reindl, A.M. Mio, C.-L. Jia, E. Ma, R. Mazzarello, M. Wuttig, W. Zhang, Genesis and effects of swapping bilayers in hexagonal GeSb2Te4, Chem. Mater. 30 (2018) 4770–4777.
[52] M. Zhu, K. Ren, L. Liu, S. Lv, X. Miao, M. Xu, Z. Song, Direct observation of partial disorder and zipperlike transition in crystalline phase change materials, Phys. Rev. Mater. 3 (2019) 033603.
[53] A. Lotnyk, M. Behrens, B. Rauschenbach, Phase change thin films for non-volatile memory applications, Nanoscale Adv. (2019), doi: 10.1039/c9na00366e.
[54] B.J. Kooi, J. Momand, High resolution imaging of chalcogenide superlattices for data storage applications: progress and prospects, Phys. Status Solidi RRL 13 (2019) 1800562.
[55] M. Wuttig, D. Lusebrink, D. Wamwangi, W. Welnic, M. Gillessen, R. Dronskowski, The role of vacancies and local distortions in the design of new phase-change materials, Nat. Mater. 6 (2007) 122–128.
[56] W. Zhang, V.L. Deringer, R. Dronskowski, R. Mazzarello, E. Ma, M. Wuttig, Density functional theory guided advances in phase-change materials and memories, MRS Bulletin 40 (2015) 856–865.
[57] P.W. Anderson, Absence of diffusion in certain random lattices, Phys. Rev. 109 (1958) 1492.
[58] M.M. Dück, T. Schäfer, S. Jakobs, C.-F. Schön, H. Niehaus, O. Cojocaru-Mirédin, M. Wuttig, Disorder control in crystalline GeSb2Te4 and its impact on characteristic length scales, Phys. Status Solidi RRL 13 (2019) 1800578.
[59] J.P. Perdew, K. Burke, M. Ernzerhof, Generalized gradient approximation made simple, Phys. Rev. Lett. 77 (1996) 3865–3868.
[60] G. Kresse, D. Joubert, From ultrasoft pseudopotentials to the projector augmented-wave method, Phys. Rev. B 59 (1999) 1758.
[61] G. Kresse, J. F., Efficient iterative schemes for ab initio total-energy calculations using a plane-wave basis set, Phys. Rev. B 54 (1996) 11169.
[62] G. Henkelman, B.P. Uberuaga, H. Jonsson, A climbing image nudged elastic band method for finding saddle points and minimum energy paths, J. Chem. Phys. 113 (2000) 9901–9904.
[63] G. Henkelman, H. Jonsson, Improved tangent estimate in the nudged elastic band method for finding minimum energy paths and saddle points, J. Chem. Phys. 113 (2000) 9978–9985.
[64] S. Grimme, J. Antony, S. Ehrlich, H. Krieg, A consistent and accurate ab initio parametrization of density functional dispersion correction (DFT-D) for the 94 elements H-Pu, J. Chem. Phys. 132 (2010) 154104.
[65] R. Wang, F.R.L. Lange, S. Cecchi, M. Hanke, M. Wuttig, R. Calarco, 2D or not 2D: strain tuning in weakly coupled heterostructures, Adv. Funct. Mater. 28 (2018) 1705901.
[66] J. Wang, I. Ronneberger, L. Zhou, L. Lu, V.L. Deringer, B. Zhang, L. Tian, H. Du, C. Jia, X. Qian, M. Wuttig, R. Mazzarello, W. Zhang, Unconventional two-dimensional germanium dichalcogenides, Nanoscale 10 (2018) 7363–7368.
[67] A.M. Mio, P.M. Konze, A. Meledin, M. Küpers, M. Pohlmann, M. Kaminski, R. Dronskowski, J. Mayer, M. Wuttig, Impact of bonding on the stacking defects in layered chalcogenides, Adv Funct Mater 29 (2019) 1902332.
[68] W. Zhang, Ab Initio Investigation of Phase Change Materials: Structural, Electronic and Kinetic properties PhD thesis. RWTH Aachen, 2014.
[69] X. Yu, J. Robertson, Modeling of switching mechanism in GeSbTe chalcogenide superlattices, Sci. Rep. 5 (2015) 12612.

[70] X. Yu, J. Robertson, Atomic layering, intermixing and switching mechanism in Ge-Sb-Te based chalcogenide superlattices, Sci. Rep. 6 (2016) 37325.
[71] D.B. Williams, C.B. Carter, Transmission Electron Microscopy A Textbook For Material Science, Springer Press, New York, 2009.
[72] T.-T. Jiang, J.-J. Wang, L. Lu, C.-S. Ma, D.-L. Zhang, F. Rao, C.-L. Jia, W. Zhang, Progressive amorphization of GeSbTe phase-change material under electron beam irradiation, APL Mater 7 (2019) 081121.
[73] S. Privitera, A.M. Mio, W. Zhang, R. Mazzarello, C. Persch, M. Wuttig, E. Rimini, Strain development and damage accumulation under ion irradiation of polycrystalline Ge-Sb-Te alloys, Nanosci. Nanotechnol. Lett. 9 (2017) 1095–1101.
[74] S.B. Fisher, On the temperature rise in electron irradiated foils, Radiat. Eff. 5 (1970) 239–243.
[75] M. Liu, L. Xu, X. Lin, Heating effect of electron beam bombardment, Scanning 16 (1994) 1–5.
[76] I. Jencic, M.W. Bench, I.M. Robertson, Electron-beam-induced crystallization of isolated amorphous regions in Si, Ge, GaP, and GaAs, J. Appl. Phys. 78 (1995) 974–982.
[77] B.J. Kooi, W.M.G. Groot, J.T.M.D. Hosson, In situ transmission electron microscopy study of the crystallization of Ge2Sb2Te5, J. Appl. Phys. 95 (2004) 924.
[78] R. Pandian, B.J. Kooi, J.T.M.D. Hosson, A. Pauza, Influence of electron beam exposure on crystallization of phase-change materials, J. Appl. Phys. 101 (2007) 053529.
[79] J. Tomforde, W. Bensch, L. Kienle, V. Duppel, P. Merkelbach, M. Wuttig, Thin films of Ge–Sb–Te-based phase change materials: microstructure and in situ transformation, Chem. Mater. 23 (2011) 3871–3878.
[80] J.-J. Wang, T.-T. Jiang, L. Tian, D.-L. Zhang, W. Zhang, Effects of electron beam irradiation on amorphous GeSbTe film, Mater. China 38 (2019) 110–115.
[81] A. Lotnyk, T. Dankwort, I. Hilmi, L. Kienle, B. Rauschenbach, In situ observations of reversible vacancy ordering process in van der Waals bonded Ge-Sb-Te thin films and GeTe-Sb2Te3 superlattices, Nanoscale 11 (2019) 10838–10845.
[82] A. Lotnyk, U. Ross, T. Dankwort, I. Hilmi, L. Kienle, B. Rauschenbach, Atomic structure and dynamic reconfiguration of layered defects in van der Waals layered Ge-Sb-Te based materials, Acta Mater 141 (2017) 92–96.
[83] A. Lotnyk, I. hilmi, U. Ross, B. Rauschenbach, Van der Waals interfacial bonding and intermixing in GeTe-Sb2Te3-based superlattices, Nano Res 11 (2017) 1676–1686.
[84] U. Ross, A. Lotnyk, E. Thelander, B. Rauschenbach, Microstructure evolution in pulsed laser deposited epitaxial Ge-Sb-Te chalcogenide thin films, J. Alloys Compd 676 (2016) 582–590.
[85] J.-J. Wang, J. Wang, Y. Xu, T. Xin, Z. Song, M. Pohlmann, M. Kaminski, L. Lu, H. Du, C.-L. Jia, R. Mazzarello, M. Wuttig, W. Zhang, Layer–Switching mechanisms in Sb2Te3, Phys. Status Solidi RRL 13 (2019) 1900320.